A reduced model for ion temperature gradient turbulent transport in helical plasmas

M. Nunami, T.-H. Watanabe, and H. Sugama

Citation: Physics of Plasmas (1994-present) **20**, 092307 (2013); doi: 10.1063/1.4822337
View online: http://dx.doi.org/10.1063/1.4822337
View Table of Contents: http://scitation.aip.org/content/aip/journal/pop/20/9?ver=pdfcov
Published by the AIP Publishing

A reduced model for ion temperature gradient turbulent transport in helical plasmas

M. Nunami,[1,2,a)] T.-H. Watanabe,[1,2] and H. Sugama[1,2]
[1]*National Institute for Fusion Science, Toki, Gifu 509-5292, Japan*
[2]*The Graduate University for Advanced Studies, Toki, Gifu 509-5292, Japan*

(Received 9 July 2013; accepted 6 September 2013; published online 25 September 2013)

A novel reduced model for ion temperature gradient (ITG) turbulent transport in helical plasmas is presented. The model enables one to predict nonlinear gyrokinetic simulation results from linear gyrokinetic analyses. It is shown from nonlinear gyrokinetic simulations of the ITG turbulence in helical plasmas that the transport coefficient can be expressed as a function of the turbulent fluctuation level and the averaged zonal flow amplitude. Then, the reduced model for the turbulent ion heat diffusivity is derived by representing the nonlinear turbulent fluctuations and zonal flow amplitude in terms of the linear growth rate of the ITG instability and the linear response of the zonal flow potentials. It is confirmed that the reduced transport model is in a good agreement with nonlinear gyrokinetic simulation results for high ion temperature plasmas in the large helical device. © *2013 AIP Publishing LLC*. [http://dx.doi.org/10.1063/1.4822337]

I. INTRODUCTION

Understanding physical mechanisms of the anomalous transport has been one of the most critical issues in researches of magnetically confined fusion plasmas for the several decades. In order to design fusion reactors, it is highly necessary to predict the turbulent transport level caused by microinstabilities such as the ion temperature gradient (ITG) mode. The nonlinear gyrokinetic simulation[1] is the first-principle-based method for evaluating the turbulent transport. Owing to recent progress in computer performance, it can be possible to perform direct numerical simulations of plasma microturbulence under realistic experimental conditions. Indeed, comparisons between gyrokinetic turbulence simulations and experiments have been made not only for tokamaks[2] but also for helical plasmas.[3]

Since the turbulence simulations require expensive computational costs, it is not practical to perform nonlinear gyrokinetic simulations a large number of times for the purpose of surveying the transport levels in a wide space of multiple parameters corresponding to various experimental conditions. Especially, gyrokinetic simulations for helical systems such as stellarators and heliotrons[4–7] tend to consume much larger computational resources than for tokamaks because of the higher spatial resolutions required by the complicated helical field structure. Therefore, it is desired to establish a reduced transport model which can quickly reproduce the nonlinear simulation results within allowable errors. Such reduced transport modeling for tokamaks has been extensively done.[8–13] For example, the GLF23 and TGLF models[10–13] employ the quasi linear transport fluxes obtained from linear gyrofluid equations and have been calibrated with nonlinear gyrokinetic simulations. For helical plasmas, so far, there have been a small number of studies on the transport modeling (see, for example, Refs. 14 and 15).

In our previous papers,[3,16] we performed gyrokinetic Vlasov simulations for ITG turbulent transport in the Large Helical Device[17] (LHD) plasma with the high ion temperature[18] by using the local flux-tube code, GKV-X.[19] In the GKV-X simulations, the nonlinear gyrokinetic equation for the perturbed ion gyrocenter distribution function[20,21] in the low-β electrostatic limit

$$\left(\frac{\partial}{\partial t}+v_{\parallel}\boldsymbol{b}\cdot\nabla+\frac{c}{B}\boldsymbol{b}\times\nabla\Phi\cdot\nabla-\frac{\mu}{m_{\mathrm{i}}}\boldsymbol{b}\cdot\nabla B\frac{\partial}{\partial v_{\parallel}}+\boldsymbol{v}_{\mathrm{d}}\cdot\nabla\right)\delta f = (\boldsymbol{v}_{*}-\boldsymbol{v}_{\mathrm{d}}-v_{\parallel}\boldsymbol{b})\cdot\frac{e\nabla\Phi}{T_{\mathrm{i}}}F_{\mathrm{M}}+C(\delta f) \tag{1}$$

is solved with assuming the adiabatic electron response. Here, the parallel velocity and the magnetic moment are denoted by $v_{\parallel}$ and $\mu = m_{\mathrm{i}}v_{\perp}^2/2B$, respectively. The magnetic and diamagnetic drift velocities are represented by $\boldsymbol{v}_{\mathrm{d}}$ and $\boldsymbol{v}_{*}$, respectively. In the simulations, the turbulent transport levels and the wavenumber spectra of the density fluctuations successfully reproduce the experimental results. From the nonlinear gyrokinetic ITG turbulent transport simulation results, we have found a simple model function to represent the ion heat diffusivity in terms of the turbulent fluctuations and the zonal flow amplitude. The model function clarifies that not only the turbulent fluctuations but also the zonal flows contribute to the ITG turbulent transport level, where the zonal flows play a significant role on the transport reduction in helical plasmas.[22,23]

In this paper, the model function is improved by including new results from nonlinear gyrokinetic simulations performed for a wide range of equilibrium parameters. Furthermore, we find that the amplitudes of the turbulent fluctuations and the zonal flows in the nonlinear simulation results are well correlated with linear simulation results on the ITG mode growth rates and the zonal flow response functions. Then, a novel reduced transport model which predicts

a)nunami.masanori@nifs.ac.jp

the turbulent ion heat diffusivity from only the linear simulation results is derived, and its validity is examined by comparing the prediction with the nonlinear simulation results.

II. RELATION AMONG TURBULENCE, ZONAL FLOW, AND TRANSPORT

It is widely known that the anomalous transport driven by the ITG turbulence is regulated by zonal flows, where the nonlinear interaction causes the spectral entropy transfer from low to high radial wavenumber regions.[24] In order to define the model function for the ITG turbulent transport level, which clarifies the relationship among the ion heat transport coefficient, the ITG turbulent fluctuations, and the zonal flows, we employ the squared turbulent potential fluctuation

$$\mathcal{T} \equiv \frac{1}{2}\sum_{k_x,k_y\neq 0}\langle|\tilde{\phi}_{k_x,k_y}|^2\rangle \tag{2}$$

and the squared zonal flow potential

$$\mathcal{Z} \equiv \frac{1}{2}\sum_{k_x}\langle|\tilde{\phi}_{k_x,k_y=0}|^2\rangle. \tag{3}$$

Here, $\tilde{\phi}$ is the normalized electrostatic potential fluctuation defined as $\tilde{\phi} = \phi/(T_i\rho_{ti}/eR_0)$. The average along the field line is denoted by $\langle\cdots\rangle$, and (k_x, k_y) represent the radial and poloidal wavenumbers. Using GKV-X, various nonlinear local simulations of the ITG turbulent transport in LHD plasmas with high ion temperature are performed at several radial positions, $\rho \equiv r/a$ with the minor radius a, in two different field configurations with the major radius $R_0 = 3.75$ m and 3.6 m. The field configuration with $R_0 = 3.75$ m corresponds to the LHD plasma #88343 investigated in Ref. 3, and the configuration with $R_0 = 3.6$ m, which has a more inward-shifted magnetic axis position, is one of the optimized configurations to reduce the neoclassical transport.[25] Based on the temperature and density profiles and field configurations obtained from the high ion temperature LHD experiments, the ion temperature gradient R_0/L_{Ti}, density gradient R_0/L_n, safety factor q, magnetic shear $\hat{s} \equiv (r/q)dq/dr$, and other parameters are varied in a realistic region of parameter space covered by high ion temperature LHD plasmas. In addition, the ion temperature gradient is artificially changed from 0.9 to 2.0 times the experimental values at $\rho = 0.5$ and 0.65. In total, we have performed twenty-one nonlinear simulations with various parameters in a range shown in Table I.

Figure 1 shows the time evolutions of $\mathcal{T}$, $\mathcal{Z}$ and the ion heat transport coefficient in the gyro-Bohm unit χ_i/χ_i^{GB} for the two cases at the same radial location $\rho = 0.65$ using the same local parameters except for the field configurations. Here, the gyro-Bohm diffusivity is defined by $\chi_i^{GB} = \rho_{ti}^2 v_{ti}/R_0$ with the ion thermal velocity $v_{ti} = \sqrt{T_i/m_i}$. For the simulation in Fig. 1, the ion temperature is given by $T_i = 2.16$ keV, and the ion thermal gyro radius is $\rho_{ti} \equiv v_{ti}/\Omega_i = 1.8 \times 10^{-3}$ m, where $\Omega_i = eB/m_i c$ represents the ion gyro frequency. Over the time window $50 < t/(R_0/v_{ti}) < 200$, the time averaged values of the turbulent fluctuation intensity $\mathcal{T}$ for the two cases are at the same level each other, which corresponds to the fact that the maximum linear growth rates of the ITG modes are almost the same, $\gamma_{max} = 0.246\, v_{ti}/R_0$ for the configuration with $R_0 = 3.75$ m and $\gamma_{max} = 0.252\, v_{ti}/R_0$ for $R_0 = 3.6$ m. On the other hand, the squared zonal flow amplitude $\mathcal{Z}$ for $R_0 = 3.6$ m is greater than twice of that for $R_0 = 3.75$ m. Consequently, by the enhanced zonal flow generation for $R_0 = 3.6$ m, the transport coefficient χ_i/χ_i^{GB} is reduced to 70% of that for $R_0 = 3.75$ m. Thus, it is expected that the transport level depends not only on the turbulent fluctuations $(\mathcal{T})$ but also on the zonal flow contributions $(\mathcal{Z})$.

TABLE I. Range of each parameter used in the simulations.

Parameter	Range
ρ	0.46 to 0.83
q	1.1 to 2.2
$\hat{s}$	−1.84 to −0.53
R_0/L_{Ti}	7.5 to 23.9
R_0/L_n	−2.04 to 0.36

In Fig. 2(a), the transport coefficients $\bar{\chi}_i/\chi_i^{GB}$ obtained from all nonlinear simulations are compared with a model function of $\bar{\mathcal{T}}$ and $\bar{\mathcal{Z}}$, where the bars represent time averages over the time window in the saturation phase for each nonlinear simulation and the width of the window is larger than 60 R_0/v_{ti}. Here, a fitting function $\mathcal{F}(\bar{\mathcal{T}}, \bar{\mathcal{Z}})$ is defined by

$$\frac{\bar{\chi}_i}{\chi_i^{GB}} = \mathcal{F}(\bar{\mathcal{T}}, \bar{\mathcal{Z}}) \equiv \frac{C_1\bar{\mathcal{T}}^{\alpha}}{C_2 + \bar{\mathcal{Z}}^{1/2}/\bar{\mathcal{T}}}, \tag{4}$$

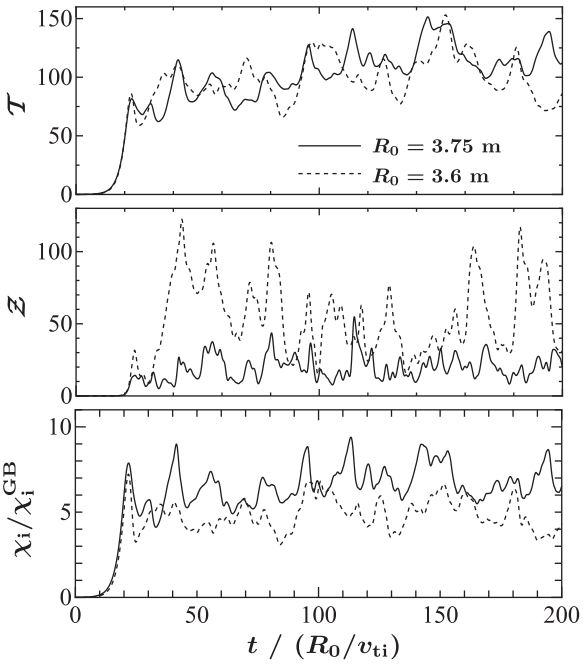

FIG. 1. Time evolutions of $\mathcal{T}$, $\mathcal{Z}$, and χ_i/χ_i^{GB} at $\rho = 0.65$ resulting from the nonlinear gyrokinetic simulations for magnetic field configurations with $R_0 = 3.75$ m and 3.6 m. Solid and dotted curves correspond to the cases for $R_0 = 3.75$ m and 3.6 m, respectively.

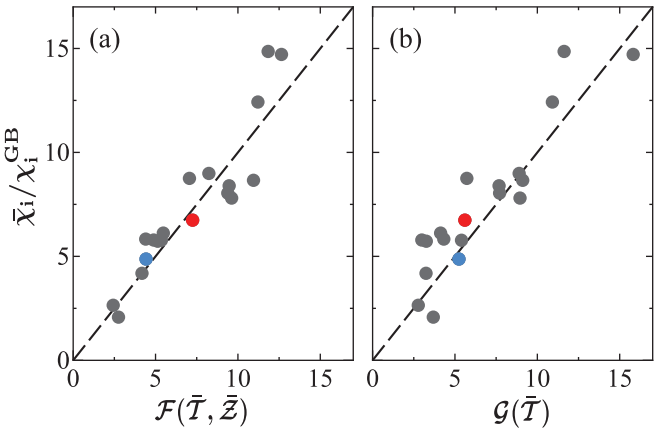

FIG. 2. Comparison of $\bar{\chi}_i/\chi_i^{GB}$ obtained from the nonlinear simulations to the functions (a) $\mathcal{F}(\bar{T},\bar{\mathcal{Z}})$ and (b) $\mathcal{G}(\bar{T})$. The functions $\mathcal{F}(\bar{T},\bar{\mathcal{Z}})$ and $\mathcal{G}(\bar{T})$ are defined by Eqs. (4) and (5), respectively. Red and blue symbols represent the results shown in Fig. 1 for $R_0 = 3.75$ m and 3.6 m, respectively.

with $\alpha = 0.38$, $C_1 = 6.3 \times 10^{-2}$ and $C_2 = 1.1 \times 10^{-2}$. In spite of wide range of parameters employed in the simulations, $\bar{\chi}_i$ is well represented by this simple form, where the numerator $C_1\bar{T}^{\alpha}$ for $\alpha > 0$ indicates the increase of χ_i with the turbulent fluctuations, while $\bar{\mathcal{Z}}^{1/2}$ in the denominator represents the transport reduction due to the zonal flow generation. If we ignore the contributions of the zonal flows to the transport coefficient, χ_i is fitted by a function of $\bar{T}$ alone as shown in Fig. 2(b) where the fitting function $\mathcal{G}(\bar{T})$ is given by

$$\mathcal{G}(\bar{T}) \equiv C_0\bar{T}^{\delta}, \tag{5}$$

with $\delta = 0.83$ and $C_0 = 0.11$. However, the function $\mathcal{G}(\bar{T})$ cannot explain the difference of the diffusivity χ_i for the two cases shown in Fig. 1. Furthermore, the relative error for fitting $\bar{\chi}_i/\chi_i^{GB}$ by $\mathcal{G}$ is larger than that by $\mathcal{F}$; $\sigma_{\mathcal{G}} = 0.269$ and $\sigma_{\mathcal{F}} = 0.159$, where σ's are defined as the root mean square of $[\bar{\chi}_i/\chi_i^{Model} - 1]$ with $\chi_i^{Model}/\chi_i^{GB} = \mathcal{G}$ and $\mathcal{F}$. Therefore, we should adopt the function $\mathcal{F}(\bar{T},\bar{\mathcal{Z}})$ rather than $\mathcal{G}(\bar{T})$ for the evaluation of the ion heat diffusivity. In Sec. III, for simplicity, the bars for the averaged values of the nonlinear quantities, $\chi_i, \mathcal{T}$ and $\mathcal{Z}$, are omitted.

III. TRANSPORT MODEL

In Sec. II, we have quantitatively evaluated the contributions of the turbulent fluctuations and the zonal flows to the transport level. Therefore, if their contributions can be represented by other simple means such as linear gyrokinetic analyses, the relation in Eq. (4) would be useful to construct a reduced transport model in helical plasmas.

Now, let us consider how to relate the nonlinear simulation results with linear simulation results. Figures 3(a) and 3(b) show the wavenumber spectra of the linear growth rates γ_k of the ITG mode divided by square of the poloidal wavenumber k_y, and those of the squared potential fluctuation $S_{\mathcal{T}}(k_y\rho_{ti}) \equiv \sum_{k_x}\langle|\tilde{\phi}_{kx,ky}|^2\rangle/\Delta\tilde{k}_y$, respectively. Here, the growth rate and wavenumber are normalized as $\tilde{\gamma} \equiv \gamma/(v_{ti}/R_0)$ and $\tilde{k} \equiv k\rho_{ti}$, respectively, and $\Delta\tilde{k}_y$ is the normalized minimum poloidal wavenumber. In the mixing length argument,[26] γ/k^2 is used to characterize the turbulent transport although we here plot $\tilde{\gamma}_k/\tilde{k}_y^2$ for comparison not directly to the transport level but to the potential fluctuation. In Fig. 3(a), the maximum values of the spectrum of $\tilde{\gamma}_k/\tilde{k}_y^2$ for the outer radial position in the case of $R_0 = 3.75$ m tend to be larger than for the inner radial positions, while the maximum values of that in the case of $R_0 = 3.6$ m are not so dependent on the radial position. These tendencies are also found in the spectral function $S_{\mathcal{T}}(k_y\rho_{ti})$ in Fig. 3(b). Thus, the nonlinear turbulence spectra are obviously correlated with the mixing length estimate γ_k/k_y^2. Figure 4 shows the relation between the turbulent fluctuation $\mathcal{T} = \int d(k_y\rho_{ti})S_{\mathcal{T}}$ and the mixing length estimate $\tilde{\gamma}_k/\tilde{k}_y^2$ integrated over $0.07 \le \tilde{k}_y \le 0.4$. It is found from the figure that $\mathcal{T}$ can be approximately given by

$$\mathcal{T} = C_{\mathcal{T}}\sum_{k_y}\frac{\tilde{\gamma}_k}{\tilde{k}_y^2}, \tag{6}$$

with the coefficient $C_{\mathcal{T}} = 9.8 \times 10^1$.

The turbulent transport level is not solely determined by the mixing length estimate calculated from the linear growth rates; the interaction between zonal flows and turbulence should also be incorporated into the reduced model as a key ingredient for the transport. The collisionless zonal flow damping, which affects the turbulent transport, is strongly influenced by the magnetic configuration of helical plasmas.[27–33] Figure 5 shows the linear zonal flow response functions defined by

$$\mathcal{R}_{k_x}(t) \equiv \frac{\langle\phi_{k_x,k_y=0}(t)\rangle}{\langle\phi_{k_x,k_y=0}(0)\rangle}, \tag{7}$$

and Fig. 6 represents radial wavenumber spectra of the squared zonal flow potential $S_{\mathcal{Z}}(k_x\rho_{ti}) \equiv \langle|\tilde{\phi}_{kx,0}|^2\rangle/\Delta\tilde{k}_x$ obtained by the nonlinear gyrokinetic simulations, where

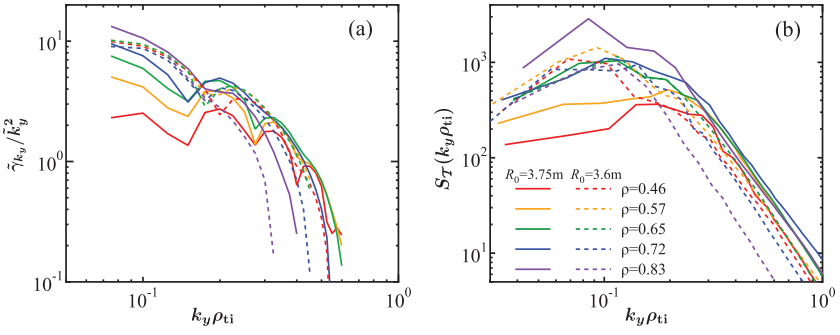

FIG. 3. Poloidal wavenumber spectra of (a) the linear ITG growth rates divided by the square of the wavenumber k_y and (b) the time averages of squared potential fluctuations $S_{\mathcal{T}}(k_y\rho_{ti}) = \sum_{k_x}\langle|\tilde{\phi}_{kx,ky}|^2\rangle/\Delta\tilde{k}_y$, at $\rho = 0.46$, 0.57, 0.65, 0.72, and 0.83 in the cases of $R_0 = 3.75$ m (solid curves) and $R_0 = 3.6$ m (dotted curves).

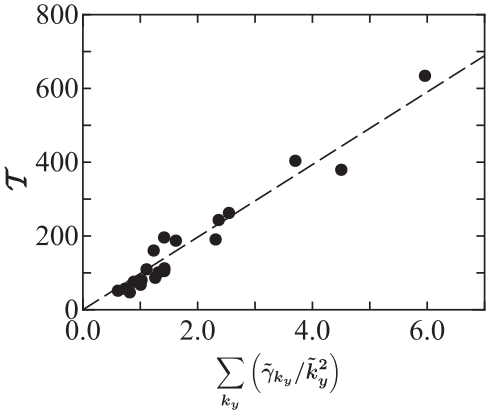

FIG. 4. The squared turbulent potential $\mathcal{T}$ versus the k_y space integral of linear growth rate of the ITG mode divided by the square of poloidal wavenumber, $\tilde{\gamma}_{ky}/\tilde{k}_y^2$.

$\Delta\tilde{k}_x$ is the normalized minimum radial wavenumber. Comparing of both figures shows that the linear response functions have a positive correlation with the squared zonal flow potential $S_{\mathcal{Z}}(k_x\rho_{\rm ti})$. For example, according to the higher response functions for $R_0 = 3.6\,\mathrm{m}$ than that for the cases with $R_0 = 3.75\,\mathrm{m}$, the zonal flow spectra $S_{\mathcal{Z}}(k_x\rho_{\rm ti})$ in the case with $R_0 = 3.6\,\mathrm{m}$ has larger value than that for $R_0 = 3.75\,\mathrm{m}$ in the low k_x region. In order to verify the correlation between the linear response functions $\mathcal{R}_{k_x}(t)$ and the zonal flow amplitude $\mathcal{Z} = \int d(k_x\rho_{\rm ti})S_{\mathcal{Z}}$ obtained from the nonlinear simulations, we employ the zonal flow *decay time*[28] defined by

$$\tau_{\rm ZF} \equiv \int_0^{\tau_{\rm f}} dt\, \mathcal{R}_{k_x}(t) \tag{8}$$

and plot the relation between the square root of the ratio of zonal flow potential to the turbulent potential, $\sqrt{\mathcal{Z}/\mathcal{T}}$, and $\tilde{\tau}_{\rm ZF} \equiv \tau_{\rm ZF}/(R_0/v_{\rm ti})$ in Fig. 7. Here, we use $\mathcal{Z}/\mathcal{T}$ instead of $\mathcal{Z}$ because the zonal flow level is determined not only by the zonal flow decay but also by the turbulence itself as a source of the zonal flow generation. In the plot, we set $\tau_{\rm f} = 25\,R_0/v_{\rm ti}$

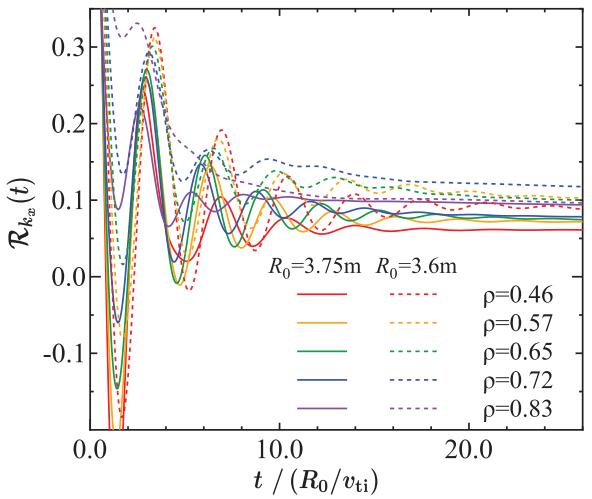

FIG. 5. Linear response functions of zonal flow potentials $\mathcal{R}_{k_x}(t) = \langle\phi_{k_x,0}(t)\rangle/\langle\phi_{k_x,0}(0)\rangle$ with $k_x\rho_{\rm ti} = 0.25$ at $\rho = 0.46$, 0.57, 0.65, 0.72, and 0.83 in the cases of $R_0 = 3.75\,\mathrm{m}$ (solid curves) and $R_0 = 3.6\,\mathrm{m}$ (dotted curves).

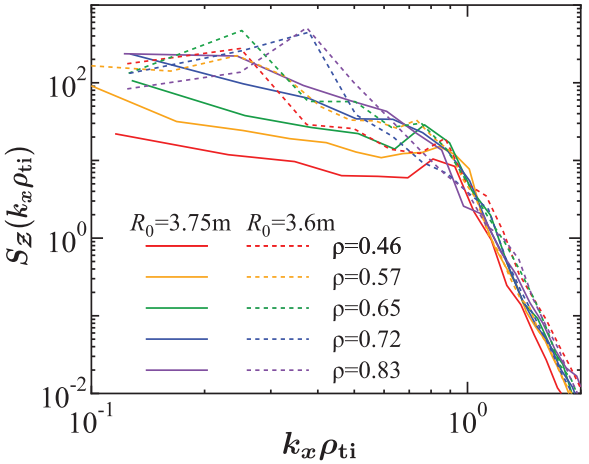

FIG. 6. Radial wavenumber spectra of the time averages of squared zonal flow potentials, $S_{\mathcal{Z}}(k_x\rho_{\rm ti}) = \langle|\tilde{\phi}_{kx,ky=0}|^2\rangle/\Delta\tilde{k}_x$, at $\rho = 0.46$, 0.57, 0.65, 0.72, and 0.83 in the cases of $R_0 = 3.75\,\mathrm{m}$ (solid curves) and $R_0 = 3.6\,\mathrm{m}$ (dotted curves).

although $\tau_{\rm ZF}$ is not significantly dependent on $\tau_{\rm f} > 25\,R_0/v_{\rm ti}$. Also, the correlation time of the turbulent sources is shorter than $25\,R_0/v_{\rm ti}$ in all cases of the nonlinear simulations as shown in Fig. 1, and thus the zonal flow response function for $\tau_{\rm f} > 25\,R_0/v_{\rm ti}$ is not considered to influence the generated zonal flow level. For the radial wavenumber, we use $k_x\rho_{\rm ti} = 0.25$ because there exist peaks of the spectra $S_{\mathcal{Z}}$ around $k_x\rho_{\rm ti} = 0.25$. We also confirmed that the difference of the collisionless decay time $\tau_{\rm ZF}$ from the collisional decay time $\tau_{\rm ZF}^{(\rm col.)}$ for the small collisionality used in the nonlinear simulation at $\rho = 0.65$ in $R_0 = 3.75\,\mathrm{m}$ case is small, namely, $|\tau_{\rm ZF} - \tau_{\rm ZF}^{(\rm col.)}|\,/\,\tau_{\rm ZF} < 0.1$, because the collision time ($\tau_{\rm col} \sim 450\,R_0/v_{\rm ti}$) used in the simulation is quite larger than $\tau_{\rm ZF}$ and γ^{-1} ($\sim 4\,R_0/v_{\rm ti}$). The efficiency of the zonal flow generation by the turbulence source increases with $\tau_{\rm ZF}$ as shown in Fig. 7 where we heuristically obtain the linear relation between $\sqrt{\mathcal{Z}/\mathcal{T}}$ and $\tau_{\rm ZF}$ as

$$\left(\frac{\mathcal{Z}}{\mathcal{T}}\right)^{1/2} = C_{\mathcal{Z}}\,\tilde{\tau}_{\rm ZF}, \tag{9}$$

with $C_{\mathcal{Z}} = 0.202$.

If we substitute the expressions in Eqs. (6) and (9) into Eq. (4), we finally obtain a reduced model which represents

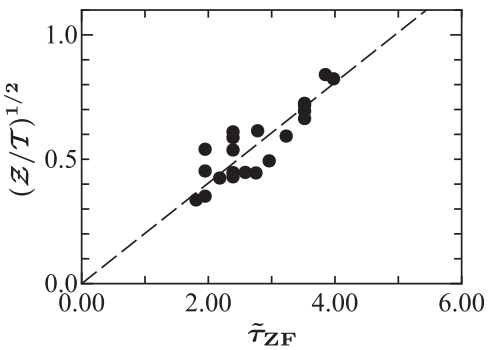

FIG. 7. The square root of the ratio of the zonal flow potential amplitude to the turbulent potential $\sqrt{\mathcal{Z}/\mathcal{T}}$ versus the normalized zonal flow decay time $\tilde{\tau}_{\rm ZF} = \int_0^{\tau_{\rm f}} dt\,\mathcal{R}_{k_x}(t)/(R_0/v_{\rm ti})$.

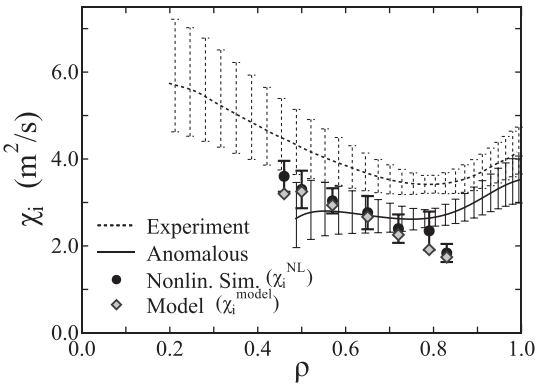

FIG. 8. Radial profiles of the ion heat diffusivity in the LHD plasma #88343 obtained from the model χ_i^{model} (diamonds) and the nonlinear GKV-X simulations χ_i^{NL} (circles). The solid curve represents the anomalous heat diffusivity obtained by subtracting the calculated neoclassical diffusivity from the experimentally obtained diffusivity (dotted curve).

the ITG turbulent ion heat diffusivity in terms of the linear simulation results

$$\frac{\chi_i^{model}}{\chi_i^{GB}} = \frac{A_1\left(\sum_k \tilde{\gamma}_k/\tilde{k}_y^2\right)^{\alpha}}{A_2 + \tilde{\tau}_{ZF}/\left(\sum_k \tilde{\gamma}_k/\tilde{k}_y^2\right)^{1/2}}, \tag{10}$$

where the coefficients are given by

$$A_1 = C_1 C_{\mathcal{T}}^{\alpha+1/2} C_{\mathcal{Z}}^{-1} = 1.8 \times 10^1, \tag{11}$$

$$A_2 = C_2 C_{\mathcal{T}}^{1/2} C_{\mathcal{Z}}^{-1} = 5.2 \times 10^{-1}. \tag{12}$$

Figure 8 shows an application of the model to the LHD high-T_i plasma #88343. It can be seen that the model predictions of the ion heat transport coefficient χ_i^{model} given in Eq. (10) agree well with the nonlinear GKV-X simulation results χ_i^{NL} within the error bars which are given as the standard deviations of the diffusivities calculated over each time window. In Fig. 9, χ_i^{NL} and χ_i^{model} are compared for all nonlinear simulation results, showing that the present model based on the linear analyses well reproduce the nonlinear gyrokinetic simulation results for a wide parameter range with the root mean square of the relative errors given by $\sigma_{model} = 0.129$. Especially, the diamond symbols in Figs. 8 and 9 represent the model results for the parameters of the LHD experiment #88343, where the model can predict the nonlinear simulation results quite accurately with the error of $\sigma_{model}^{\#88343} = 0.104$. By the way, if we construct the other model $\chi_i^{\mathcal{G}}$ from the function $\mathcal{G}$ in Eq. (5) and the relation Eq. (6) as $\chi_i^{\mathcal{G}}/\chi_i^{GB} = A_0(\sum_k \tilde{\gamma}_k/\tilde{k}_y^2)^{\delta}$ with $A_0 = C_0 C_{\mathcal{T}}^{\delta} = 5.1$, the relative errors become larger ($\sigma_{\mathcal{G}-model} = 0.307$ and $\sigma_{\mathcal{G}-model}^{\#88343} = 0.365$).

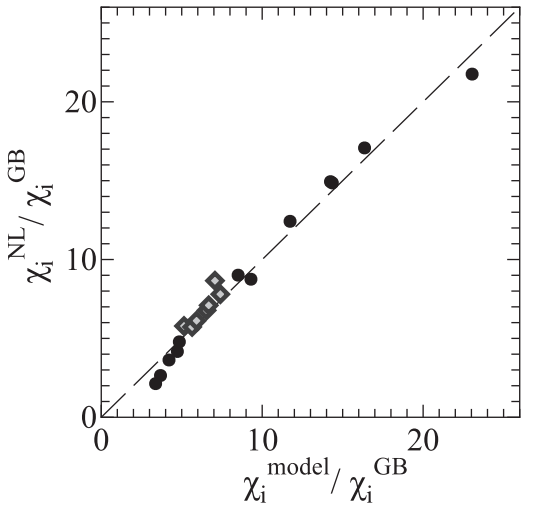

FIG. 9. Comparison of the ion heat diffusivities between the nonlinear simulation results χ_i^{NL} and the model predictions χ_i^{model}. Diamonds show the results in the LHD plasma #88343 shown in Fig. 8.

IV. CONCLUSIONS

Based on nonlinear gyrokinetic ITG turbulent transport simulations, we have constructed a reduced model for the ion heat turbulent transport in the LHD plasmas with high ion temperatures. We have shown that the ion heat diffusivity has a functional dependence on the amplitudes of turbulent fluctuations and zonal flows in the nonlinear simulation results and that these amplitudes are well correlated with linear simulation results on the ITG modes and zonal flows. Using these properties, we have derived the reduced transport model which expresses the turbulent heat diffusivity in terms of the linear growth rates of the ITG mode and the linear response functions of the zonal flow potentials. The nonlinear gyrokinetic transport simulation results are quantitatively reproduced by the model calculations. Since the computational cost of the present model is extremely smaller than that of the nonlinear simulation (the ratio is less than 5%), the model can be applied to an integrated transport code for helical plasmas such as TASK3D.[34] The present model is applicable to only collisionless or weakly collisional cases because it is derived from results of the nonlinear simulations in which collisional effects on the ITG mode growth rate and the zonal flow decay time are negligibly small. Since the number of samples used here is still too limited to verify the validity of the model for more general cases, it will be improved in the future by performing further extensive nonlinear simulations to investigate effects of other instability sources such as trapped electron modes (TEMs) as well as dependencies on collisionality, field configurations for different devices, and profiles of temperatures and densities.

ACKNOWLEDGMENTS

M.N. would like to thank Dr. M. Nakata for useful discussions. This work was supported in part by the Japanese Ministry of Education, Culture, Sports, Science and Technology (Grant Nos. 22760660, 21560861, and 24561030), by National Institute for Fusion Science (NIFS) Collaborative Research Program (KNST039, KNXN229, and KNTT015), and by use of Helios system at International Fusion Energy Research Center (Project code: VLDGK_ST and GTNAXIS). Part of the results is obtained by using the K computer at the RIKEN Advanced Institute for Computational Science (Proposal No. hp120138).

[1]X. Garbet, Y. Idomura, L. Villard, and T. H. Watanabe, Nucl. Fusion **50**, 043002 (2010).
[2]T. L. Rhodes, C. Holland, S. P. Smith, A. E. White, K. H. Burrell, J. Candy, J. C. DeBoo, E. J. Doyle, J. C. Hillesheim, J. E. Kinsey, G. R. McKee, D. Mikkelsen, W. A. Peebles, C. C. Petty, R. Prater, S. Parker, Y. Chen, L. Schmitz, G. M. Staebler, R. E. Waltz, G. Wang, Z. Yan, and L. Zeng, Nucl. Fusion **51**, 063022 (2011).
[3]M. Nunami, T.-H. Watanabe, H. Sugama, and K. Tanaka, Phys. Plasma **19**, 042504 (2012).
[4]H. E. Mynick, Phys. Plasmas **13**, 058102 (2006).
[5]P. Xanthopoulos, F. Merz, T. Görler, and F. Jenko, Phys. Rev. Lett. **99**, 035002 (2007).
[6]J. A. Baumgaertel, G. W. Hammett, D. R. Mikkelsen, M. Nunami, and P. Xanthopoulos, Phys. Plasmas **19**, 122306 (2012).
[7]J. A. Baumgaertel, G. W. Hammett, and D. R. Mikkelsen, Phys. Plasmas **20**, 022305 (2013).
[8]M. Kotschenreuther, W. Dorland, M. A. Beer, and G. W. Hammett, Phys. Plasmas **2**, 2381 (1995).
[9]J. Weiland, *Collective Modes in Inhomogeneous Plasmas* (IOP, Britol, 2000).
[10]R. E. Waltz, G. M. Staebler, W. Dorland, G. W. Hammett, M. Kotschenreuther, and J. A. Konings, Phys. Plasmas **4**, 2482 (1997).
[11]G. M. Staebler, J. E. Kinsey, and R. E. Waltz, Phys. Plasmas **12**, 102508 (2005).
[12]G. M. Staebler, J. E. Kinsey, and R. E. Waltz, Phys. Plasmas **14**, 055909 (2007).
[13]J. E. Kinsey, G. M. Staebler, and R. E. Waltz, Phys. Plasmas **15**, 055908 (2008).
[14]W. Guttenfelder, J. Lore, D. T. Anderson, F. S. B. Anderson, J. M. Canik, W. Dorland, K. M. Likin, and J. N. Talmadge, Phys. Rev. Lett. **101**, 215002 (2008).
[15]H. E. Mynick, N. Pomphrey, and P. Xanthopoulos, Phys. Rev. Lett. **105**, 095004 (2010).
[16]M. Nunami, T.-H. Watanabe, and H. Sugama, Plasma Fusion Res. **8**, 1203019 (2013).
[17]A. Komori, H. Yamada, S. Imagawa, O. Kaneko, K. Kawahata, K. Mutoh, N. Ohyabu, Y. Takeiri, K. Ida, T. Mito, Y. Nagayama, S. Sakakibara, R. Sakamoto, T. Shimozuma, K. Y. Watanabe,O. Motojima, and LHD Experiment Group, Fusion Sci. Technol. **58**, 1 (2010).
[18]K. Tanaka, C. Michael, L. Vyacheslavov, H. Funaba, M. Yokoyama, K. Ida, M. Yoshinuma, K. Nagaoka, S. Murakami, A. Wakasa, T. Ido, A. Shimizu, M. Nishiura, Y. Takeiri, O. Kaneko, K. Tsumori, K. Ikeda, M. Osakabe, K. Kawahata, and LHD Experiment Group, Plasma Fusion Res. **5**, S2053 (2010).
[19]M. Nunami, T.-H. Watanabe, and H. Sugama, Plasma Fusion Res. **5**, 016 (2010).
[20]T.-H. Watanabe and H. Sugama, Nucl. Fusion **46**, 24 (2006).
[21]E. A. Frieman and L. Chen, Phys. Fluids **25**, 502 (1982).
[22]T.-H. Watanabe, H. Sugama, and S. Ferrando-Margalet, Phys. Rev. Lett. **100**, 195002 (2008).
[23]P. Xanthopoulos, A. Mishchenko, P. Helander, H. Sugama, and T.-H. Watanabe, Phys. Rev. Lett. **107**, 245002 (2011).
[24]M. Nakata, T.-H. Watanabe, and H. Sugama, Phys. Plasmas **19**, 022303 (2012).
[25]S. Murakami, A. Wakasa, H. Maaßberg, C. D. Beidler, H. Yamada, K. Y. Watanabe, and LHD Experimental Group, Nucl. Fusion **42**, L19 (2002).
[26]J. Wesson, *Tokamaks Second Edition* (Oxford University Press, 1997), p. 198.
[27]H. Sugama and T.-H. Watanabe, Phys. Plasma **13**, 012501 (2006).
[28]S. Ferrando-Margalet, H. Sugama, and T.-H. Watanabe, Phys. Plasma **14**, 122505 (2007).
[29]T.-H. Watanabe, H. Sugama, and S. Ferrando-Margalet, Nucl. Fusion **47**, 1383 (2007).
[30]A. Mishchenko, P. Helander, and A. Könies, Phys. Plasmas **15**, 072309 (2008).
[31]R. Kleiber, R. Hatzky, and A. Mishchenko, Contrib. Plasma Phys. **50**, 766 (2010).
[32]P. Helander, A. Mishchenko, R. Kleiber, and P. Xanthopoulos, Plasma Phys. Controlled Fusion **53**, 054006 (2011).
[33]E. Sánchez, R. Kleiber, R. Hatzky, M. Borchardt, P. Monreal, F. Castejón, A. López-Fraguas, X. Sáez, J. L. Velasco, I. Calvo, A. Alonso, and D. López-Bruna, Plasma Phys. Controlled Fusion **55**, 014015 (2013).
[34]M. Yokoyama, A. Wakasa, R. Seki, M. Sato, S. Murakami, C. Suzuki, Y. Nakamura, A. Fukuyama, and LHD Experiment Group, Plasma Fusion Res. **7**, 2403011 (2012).